JACS
JOURNAL OF THE AMERICAN CHEMICAL SOCIETY
Article
pubs.acs.org/JACS

Optical Anisotropy of Black Phosphorus in the Visible Regime

Nannan Mao,[†] Jingyi Tang,[‡] Liming Xie,[§] Juanxia Wu,[†] Bowen Han,[†] Jingjing Lin,[†] Shibin Deng,[†] Wei Ji,[∥] Hua Xu,[⊥] Kaihui Liu,[‡] Lianming Tong,[*,†] and Jin Zhang[*,†]

[†]Center for Nanochemistry, Beijing National Laboratory for Molecular Sciences, Key Laboratory for the Physics and Chemistry of Nanodevices, State Key Laboratory for Structural, Chemistry of Unstable and Stable Species, College of Chemistry and Molecular Engineering and [‡]State Key Laboratory for Mesoscopic Physics, Collaborative Innovation Center of Quantum Matter, School of Physics, Peking University, Beijing 100871, PR China

[§]Key Laboratory of Standardization and Measurement for Nanotechnology of Chinese Academy of Sciences, National Center for Nanoscience and Technology, Beijing 100190, PR China

[∥]Department of Physics and Beijing Key Laboratory of Optoelectronic Functional Materials & Micro-nano Devices, Renmin University of China, Beijing 100872, PR China

[⊥]School of Materials Science and Engineering, Shaanxi Normal University, Xi'an, 710062, PR China

Supporting Information

ABSTRACT: The striking in-plane anisotropy remains one of the most intriguing properties for the newly rediscovered black phosphorus (BP) 2D crystals. However, because of its rather low-energy band gap, the optical anisotropy of few-layer BP has been primarily investigated in the near-infrared (NIR) regime. Moreover, the essential physics that determine the intrinsic anisotropic optical property of few-layer BP, which is of great importance for practical applications in optical and optoelectronic devices, are still in the fancy of theory. Herein, we report the direct observation of the optical anisotropy of few-layer BP in the visible regime simply by using polarized optical microscopy. On the basis of the Fresnel equation, the intrinsic anisotropic complex refractive indices ($n-i\kappa$) in the visible regime (480−650 nm) were experimentally obtained for the first time using the anisotropic optical contrast spectra. Our findings not only provide a convenient approach to measure the optical constants of 2D layered materials but also suggest a possibility to design novel BP-based photonic devices such as atom-thick light modulators, including linear polarizer, phase plate, and optical compensator in a broad spectral range extending to the visible window.

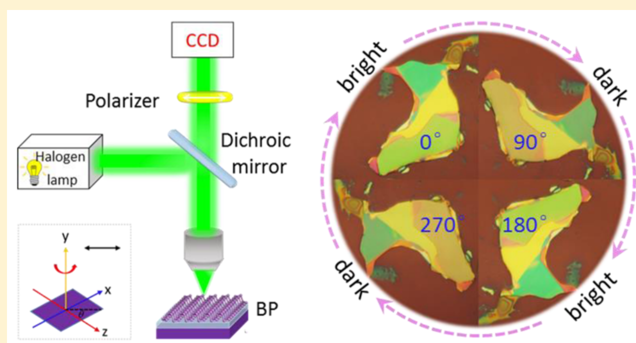

INTRODUCTION

Inspired by the fascinating properties of graphene and the layered transition metal dichalcogenides (TMDs),[1−10] scientists have been making great efforts to pursue new functional layered semiconductors.[11,12] Recently, black phosphorus (BP) has been rediscovered as a new 2D layered material because of its remarkable electronic and optical properties, such as its high carrier mobility[13−15] and tunable direct band gap.[14,16,17] Particularly, the puckered structure of BP, resulted from the sp^3 nonequivalent hybridization of each P atom, leads to the robust in-plane anisotropy nature of BP layers, including remarkable optical, electrical, and mechanical anisotropic properties.[16−27] The emergence of these anisotropic properties has stimulated the exploration of novel BP-based electronic and optical devices. Among these, the anisotropic optical property greatly facilitates BP toward functional optoelectronics because optical anisotropy supplies another degree of freedom for scientists to design and modulate the efficient optical and optoelectronic nanodevices. A fundamental understanding on the optical anisotropy of few-layer BP is therefore essential to reveal the photoelectron interaction in BP-related optoelectronics.

The visible regime is always the most commonly used optical window for practical optoelectronics. However, because of its rather low-energy band gap,[17,19] the investigation for the optical anisotropy of few-layer BP has been primarily limited in the near-infrared (NIR) regime.[18,20,28] Despite extensive theoretical predictions,[19,21,29−32] the experimental investigation on the optical anisotropy of BP in the visible regime is still missing, let alone the measurement of the complex optical constants of few-layer BP. Though it is essential for designing conceptually novel electronic and optical devices based on the optical anisotropy of BP, the accurate determination of this key parameter is rather difficult because of two facts: (i) the micrometer and nanometer size of the BP layers obtained using present methods (mechanical exfoliation, liquid phase exfoliation, etc.)[17,20,33,34] that directly hinders the measurement through

Received: October 13, 2015
Published: December 15, 2015

ACS Publications © 2015 American Chemical Society

DOI: 10.1021/jacs.5b10685
J. Am. Chem. Soc. 2016, 138, 300−305

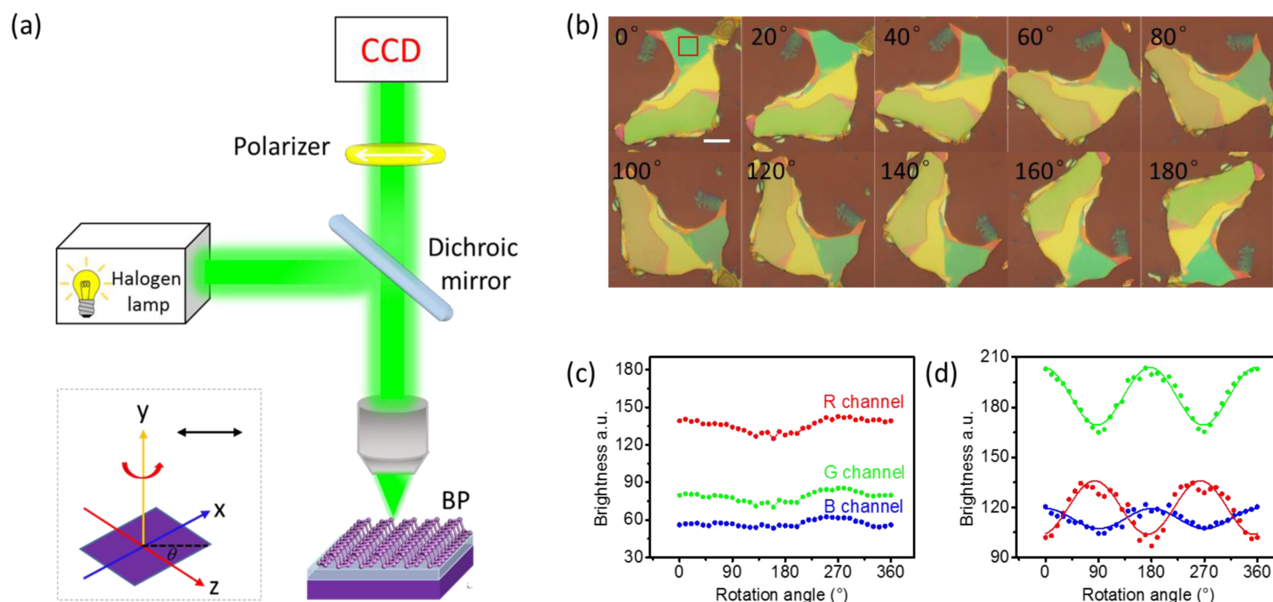

Figure 1. Schematic diagram of polarized optical imaging of BP. (a) Experimental setup of the polarized optical microscope. The inset shows the crystallographic axes (x and z corresponding to ZZ and AC directions, respectively) and the direction of the analyzer polarization (black double arrow). θ is the angle between the direction of the analyzer polarization and z (AC) axis. (b) Optical images of a thick BP sample as a function of rotation angle. The scale bar is 10 μm. RGB optical brightness of the reflected light (c) from the blank 300 nm SiO_2/Si substrate and (d) BP sample in the region marked with the red square in b.

conventional approaches such as spectroscopic ellipsometry technique[35,36] and (ii) the optical anisotropic complexity of biaxial BP crystal itself.[37]

Herein, by using polarized optical microscopy and spectroscopy, we report the direct observation of significant optical anisotropy of BP in the visible regime, and on the basis of the Fresnel reflection theory, the anisotropic optical constants of few-layer BP in the visible regime (480−650 nm) were experimentally obtained for the first time from the anisotropic optical contrast spectra. It turns out that 5 nm thick BP shows an apparently distinct complex refractive index especially in the range of 450−580 nm, demonstrating its strong optical anisotropy in the visible regime. The determination of the anisotropic optical constants of few-layer BP and other anisotropic 2D materials in general is of fundamental importance and may boost their applications in novel optical and optoelectronic nanodevices.

■ EXPERIMENTAL SECTION

BP samples were prepared by mechanical cleavage method from bulk BP crystals (Smart Elements) on two kinds of substrate: fused silica and Si substrate with 300 nm oxide layer. The thickness of BP samples was determined by atomic force microscopy (AFM, Dimension 3100). High-resolution transmission electron microscope (HRTEM) images of the BP samples were acquired through transmission electron microscopy (TEM, Tecnai F20, FEI). An Olympus (BX51) optical microscope with a normal white light source (tungsten halogen lamp, excitation range from 350 to 850 nm) was used for the optical contrast measurements. The angle-resolved optical contrast was measured with an analyzer placed in the light collection path in front of the detector (DP71 camera). All the spectra were measured under parallel polarizations. The optical contrast spectra and Raman spectra were recorded using a JY Horiba HR800 Raman system. The laser wavelength for Raman excitation was 632.8 nm, and the laser power was less than 100 μW. A 600/mm grating and a 100× objective lens with NA = 0.9 were used to collect reflected light and Raman signals. The actual thickness of SiO_2 layer on Si substrate was determined by spectroscopic ellipsometer (SE 850 DUV), covering a wide spectral range from 190 to 2500 nm.

■ RESULTS AND DISCUSSION

Figure 1a shows the experimental setup of the polarized optical microscope for contrast measurements. The white light (halogen lamp) was used to illuminate the BP sample. An analyzer was placed in the collection light path in front of the CCD detector, and the polarization direction of the collected signal was kept the same while the sample was rotated for angle-resolved optical imaging. The rotation angle θ is defined as the angle between the z axis of the sample and the polarization of the analyzer (inset in Figure 1a). Figure 1b shows a series of the optical images of a thick BP sample mechanically exfoliated on the 300 nm SiO_2/Si substrate at different rotation angles from 0 to 180°. It is apparent that the optical brightness of BP changes significantly with the rotation angle; see for example the area highlighted by the red rectangle. It can be clearly seen that the green color of BP at 0 and 180° is much brighter than that at 90°. To analyze quantitatively the variation, we extracted the averaged red-green-blue (RGB) values from the pictures in Figure 1b. The corresponding spectral ranges for our CCD (Olympus DP71) are 400−520 nm for B, 470−610 nm for G, and 570−700 nm for R.[38] Interestingly, we found that the intensities of RGB channels for the thick BP sample change in a periodic fashion (as shown in Figure 1c,d), whereas that of the blank SiO_2/Si substrate remains almost constant. Furthermore, the R and G/B channels show opposite variation behaviors. At 0°, the intensities for the G and B channels are maximum, whereas it is the minimum for the R channel. After the sample was rotated by 90°, the G and B channels become minimum, and the R channel is the maximum. For the rather thick BP sample, the RGB values directly represent the averaged reflection from the interface between the BP surface and air. Such results strongly indicated the optical anisotropy of BP in the visible regime.

DOI: 10.1021/jacs.5b10685
J. Am. Chem. Soc. 2016, 138, 300−305

To study quantitatively the optical anisotropy of BP, we measured the angular optical contrast of a few-layer BP sample on the 300 nm SiO_2/Si substrate. Figure 2a shows the atomic force microscopy (AFM) image of the BP sample, and the thickness was measured to be ∼7.5 nm, corresponding to 12−13 layers. The inset shows the corresponding optical image of this BP sample. The Raman spectrum with the three characteristic Raman modes of BP, that is, A^1_g (363 cm^{-1}), B_{2g} (440 cm^{-1}), and A^2_g (467 cm^{-1}), is shown in Figure 2b. The optical contrast (C_λ) is the fractional change of reflection because of the presence of the sample on a substrate, and is defined by

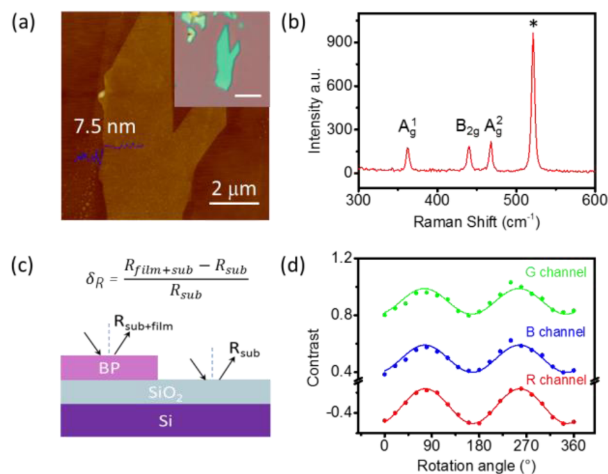

Figure 2. Anisotropic optical contrast of few-layer BP on 300 nm SiO_2/Si substrate. (a) Atomic force micrograph of a few-layer BP sample with the thickness of 7.5 nm. The inset is the optical image of this sample; the scale bar is 5 μm. (b) Typical Raman spectrum of the BP sample. The three characteristic Raman bands are A^1_g (363 cm^{-1}), B_{2g} (440 cm^{-1}) and A^2_g (467 cm^{-1}). The Raman band of silicon (ca. 520 cm^{-1}) is marked with the asterisk. (c) Sketch map for optical contrast calculation. $R_{film+sub}$ and R_{sub} are the reflected intensities from BP and blank substrate, respectively. (d) Measured optical contrast of the few-layer BP in RGB channels as a function of the rotation angle.

$$C_\lambda = \frac{R_{film+sub} - R_{sub}}{R_{sub}} \quad (1)$$

where $R_{film+sub}$ and R_{sub} are the reflected intensities collected from the sample and the blank substrate, respectively, as shown by the scheme in Figure 2c. The averaged optical contrast of the BP sample was thus calculated in the RGB channels and plotted in Figure 2d. The periodic variation was reproduced (compared to Figure 1d) because the contrast is directly related to the reflected intensity. It can also be seen that the contrast of the G and B channels are positive, whereas that for the R channel is negative, indicating that for long (red) wavelengths, the reflection collected from the BP is actually smaller than that from the blank substrate. If the few-layer BP is exfoliated on fused silica where multilayer reflection interference does not occur, then the same periodic change of optical contrast was also observed; however, the averaged contrasts for the R and G channels were rather weak (Figure S1). The periodic change of the optical contrast is an evident indication of the optical anisotropy of few-layer BP.

Interestingly, the difference in the rotation angle between the appearance of the maximums and minimums is 90°, coinciding with the angle made by the two crystalline directions of BP, that is, the ZZ and AC directions. Our previous work has demonstrated a simple approach for identifying the crystalline orientation of BP using angle-resolved polarized Raman spectroscopy (ARPRS).[25] Here we show that the crystalline orientation can also be easily identified using the angular dependence of optical contrast with even greater convenience. Figure 3b shows the recorded Raman spectra at different

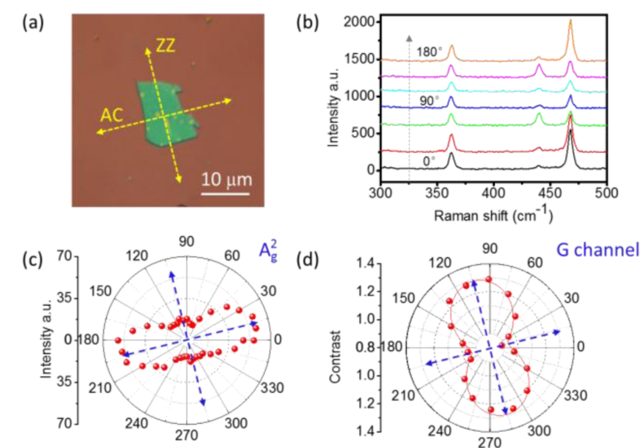

Figure 3. Crystalline orientation identification using angle-dependent optical contrast. (a) Optical image of few-layer BP on 300 nm SiO_2/Si substrate. The dashed double arrows indicate the identified AC and ZZ directions by using angle-dependent optical contrast of this sample. (b) Raman spectra of BP sample with different rotation angles. Polar plot of (c) A_g^2 Raman band and (d) optical contrast of the few-layer BP in G channel as a function of rotation angle.

rotation angles under parallel polarization configuration. The intensities of the three Raman modes vary periodically when the sample was rotated, consistent with literature.[14−16] The polar plot of the A_g^2 mode in Figure 3c shows the maximum at ∼15°, which can be identified as the AC direction of the BP sample. Accordingly, the ZZ direction is perpendicular to AC and is along the second maximum at ∼105°. Meanwhile, the polar plot of the angle-dependent optical contrast of BP is shown in Figure 3d. Apparently, the direct comparison with ARPRS results in Figure 3c strongly indicates that the maximum of optical contrast is indeed along the ZZ direction of BP. The identification was further supported by our high-resolution TEM characterizations (Figure S2).

Because the optical contrast of the atomically thin layer is the function of the dielectric constant of the material,[39−43] we derived the anisotropic refractive indices of BP on 300 nm SiO_2/Si substrate on the basis of the Fresnel equation and classical electrodynamic simulations. The transfer matrix method was chosen because of its simplicity; a single matrix can be used to quantitatively describe the reflection, refraction, and transmission through multi-dielectric layers, particularly suitable for our system of few-layered BP on 300 nm SiO_2/Si substrate.[39,42,44] The scheme is shown in Figure 4a,b. For isotropic media such as graphene, the s (electric-field vector *E* perpendicular to the plane of incidence) and p (*E* parallel to the plane of incidence) components of the incident electromagnetic waves are regarded as independent from each other. As a result, a single 2 × 2 matrix can be used to calculate the transmission and absorption of s and p components independently.[41] However, BP is one type of biaxial crystals; in other words, the dielectric constants along its three principle crystal axes are different. Thus, the situation becomes more

DOI: 10.1021/jacs.5b10685
J. Am. Chem. Soc. 2016, 138, 300−305

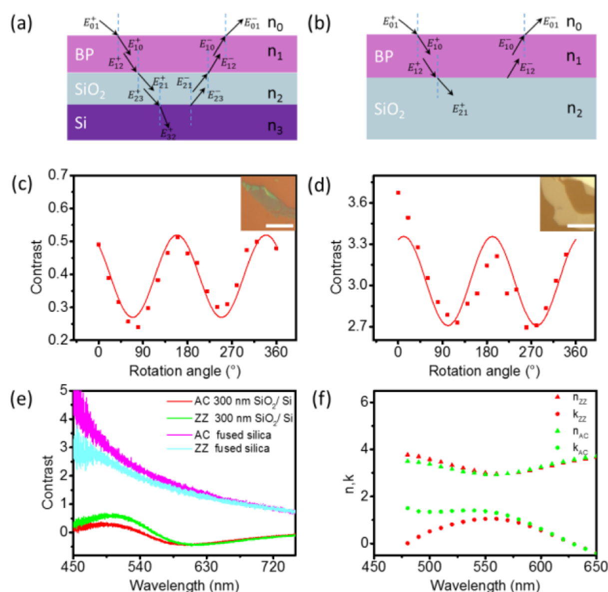

Figure 4. Simulated and measured anisotropic optical contrast and refractive indices for few-layer BP on 300 nm SiO_2/Si and fused silica substrate. Optical reflection and transmission schematic for multithin films system: (a) BP on 300 nm SiO_2/Si and (b) fused silica. n stands for the refractive index of different media: air (n_0), BP (n_1), SiO_2 (n_2) and Si (n_3). Angle-dependent optical contrast of (c) the 5 nm BP samples on 300 nm SiO_2/Si and (d) fused silica under parallel polarizations. The wavelength of the incident light is 480 nm. Solid curves are fitted results using simulated equation. Insets are the corresponding optical images of the BP samples. The scale bar is 10 μm. (e) Optical contrast spectra along AC and ZZ crystalline direction of 5 nm thick BP on 300 nm SiO_2/Si and fused silica substrates, respectively. (f) Measured refractive indices for 5 nm thick BP along AC and ZZ crystalline directions. The solid triangles and dots are the real and imaginary parts of the refractive indices, respectively.

complex, especially when the coupling between the s and p components (in practice, due to the numerical aperture of the objective lens and the cone geometry of the focused light) is taken into account.[37] For simplicity and to avoid loss of generality, we assume normal incidence. The angle between the polarization direction of the incident light and the AC crystalline axis of BP is defined as θ, as shown in Figure 1a.

Because of the birefringence of BP crystals, the incident polarized light is split into x and z polarized components along the two principle crystal axes (ZZ and AC) of BP, which travel at different velocities. Hereafter, the z component, $\overrightarrow{E_z}(y, t) = E_0 \cos \theta$, is treated as the p-polarized branch, whereas the x component, $\overrightarrow{E_x}(y, t) = E_0 \sin \theta$, is regarded as the s-polarized branch. It can be easily derived that under the normal incidence these two components will pass through the multiple medium separately without coupling. The schematic of the p-polarized component is shown in Figure 4a and consists of four media: air, BP, SiO_2, and Si. Figure 4b shows the corresponding schematic of BP on fused silica. To show the light path more clearly, we chose the oblique incidence in the schematic diagram. In Figure 4a,b, $E_{ij}^{\pm}$ is the electric field in the ith medium at the $i-j$ interface, and the superscript $\pm$ stands for the directions of the incident/reflected light. By applying the electromagnetic field boundary conditions at each interface between two different media, the relationship between the four electric fields (E_{ij}^{+}, E_{ij}^{-}, E_{ji}^{+}, and E_{ji}^{-}) is described as

$$\begin{bmatrix} E_{ij}^{+} \\ E_{ij}^{-} \end{bmatrix} = \frac{1}{t_{ij}} \begin{bmatrix} 1 & r_{ij} \\ r_{ij} & 1 \end{bmatrix} \begin{bmatrix} E_{ji}^{+} \\ E_{ji}^{-} \end{bmatrix} \quad (2)$$

where $t_{ij} = (2n_0 \cos \theta_0)/(n_0 \cos \theta_0 + n_1 \cos \theta_1)$ and $r_{ij} = (n_0 \cos \theta_0 - n_1 \cos \theta_1)/(n_0 \cos \theta_0 + n_1 \cos \theta_1)$ are the transmission and reflection coefficients at the $i-j$ interface, respectively. In the same medium, the relationship between the four electric fields at the upper and bottom interfaces can be written as

$$\begin{bmatrix} E_{ij}^{+} \\ E_{ij}^{-} \end{bmatrix} = \begin{bmatrix} e^{i\delta_i} & 0 \\ 0 & e^{-i\delta_i} \end{bmatrix} \begin{bmatrix} E_{ij+2}^{+} \\ E_{ij+2}^{-} \end{bmatrix} \quad j = 1, 2 \quad (3)$$

where $\delta_i = 2\pi \tilde{n}_i d_i/\lambda$ is the phase factor. Hence, the final formula that describes the incident and reflected electric fields on the multiple-layered media can be expressed by

$$\begin{bmatrix} E_{01}^{+} \\ E_{01}^{-} \end{bmatrix} = \frac{1}{t_{01}t_{12}t_{23}} \begin{bmatrix} 1 & r_{01} \\ r_{01} & 1 \end{bmatrix} \begin{bmatrix} e^{i\delta_1} & r_{12}e^{i\delta_1} \\ r_{12}e^{-i\delta_1} & e^{-i\delta_1} \end{bmatrix} \times \begin{bmatrix} e^{i\delta_2} & r_{12}e^{i\delta_2} \\ r_{12}e^{-i\delta_2} & e^{-i\delta_2} \end{bmatrix} \begin{bmatrix} E_{32}^{+} \\ 0 \end{bmatrix} \quad (4)$$

The ratio between the reflected and incident electric fields is the reflectivity, which can be obtained through $r_p = (E_{01}^{-}/E_{01}^{+})$. For the p-polarized (along AC direction) electric magnetic wave, the reflected electric field can be expressed by $E_{AC} = E_{01}^{-} = r_p E_{01}^{+}$. Similarly, we can get the reflected s-polarized (along ZZ direction) electric field E_{ZZ}. Because of the birefringence property of BP, the two orthogonal components of the polarized light will exit the sample with a phase difference. Therefore, the final intensity of the reflected light I under parallel polarization at sample rotation angle θ can be obtained by the interference of p- and s-polarized components in the direction of the collection polarization, expressed as follows:

$$I_{\text{film+sub}} = (E_{ZZ} \sin \theta)^2 + (E_{AC} \cos \theta)^2 + 2\sqrt{(E_{ZZ} \sin \theta)^2 \times (E_{AC} \cos \theta)^2} \cos \delta \quad (5)$$

δ is the phase difference between p- and s-polarized components. Accordingly, the intensity of the reflected light from the black SiO_2 substrate I_{sub} can also be calculated in the similar way by only considering the air, 300 nm SiO_2, and Si trilayers. Hence, the optical contrast of BP on 300 nm SiO_2/Si and fused silica substrate (Figure 4b) can be finally calculated.

Using eq 1, we then simulated the optical contrast of few-layer BP at different rotation angles. The measured optical contrasts on SiO_2/Si and fused silica substrate at 480 nm were shown in Figure 4c,4d, respectively. The solid curves are the fitting results using

$$C_\lambda = (a \sin(\theta - \varphi))^2 + (b \cos(\theta - \varphi))^2 + 2\sqrt{(a \sin(\theta - \varphi))^2 \times (b \cos(\theta - \varphi))^2} \cos \delta \quad (6)$$

where a and b are constants and θ is the polarization angle with respect to the 0° reference direction. φ is the angle between the AC direction and the 0° reference. As mentioned above, δ is the phase difference between p- and s-polarized components. The wavelength-dependent refractive indices of SiO_2 (n_2) and Si (n_3) were taken from ref 29.[45] The thickness of oxidation layer on Si substrate was 295.7 nm, measured by spectroscopic

DOI: 10.1021/jacs.5b10685
J. Am. Chem. Soc. 2016, 138, 300−305

ellipsometer. The theoretical refractive index of bulk BP calculated using density functional theory (DFT) from ref 7 was used.[19] The periodical variation of the calculated angle-dependent optical contrast of 10L BP on 300 nm SiO_2/Si substrate under 500 nm incident light illumination was well-reproduced. It is seen that our simulation agrees well with the experimental results (Figure S3).

Using the above simulations, we further show that we can obtain the experimental anisotropic refractive indices of few-layer BP from the optical contrast spectra along AC and ZZ directions. We notice that the refractive index of BP is the only unknown parameter and it contains two independent components, n and κ. To solve for the experimental values of n and κ, two sets of data are needed. We then measured the optical contrast spectra of few-layer BP on both SiO_2/Si and fused silica along AC and ZZ directions, respectively, which are plotted in Figure 4e. Figure 4c,d shows the angular-dependent optical contrast of BP on these two substrates at 480 nm. AFM measurements were carried out immediately after the BP layer is identified using optical microscope, which indicate that the thicknesses of the two BP samples are 5.0 and 5.3 nm, respectively (Figure S4). For both of the two samples, the crystalline orientations were identified using ARPRS/anisotropic contrast, as described in Figure 3. In Figure 4e, noticeable differences of the optical contrast along two crystalline orientations are clearly seen, especially in the wavelength range from 450 to 580 nm.

Combining eqs 1 and 5, the real and imaginary parts of the wavelength-dependent refractive index for 5 nm thick BP layer can be obtained at each wavelength and are plotted in Figure 4f. A significant difference between AC and ZZ directions is seen, indicating intrinsically large optical anisotropy of BP crystals in the visible regime. The real part is larger along the ZZ direction than that along the AC direction below 570 nm and becomes slightly smaller when the wavelength is above 570 nm. Additionally, the imaginary part along AC direction is always larger than that along ZZ direction. These results are reasonably comparable to the reported theoretical values on the linear dichroism of BP (Figure S5).[19,21,23] Now we turn back to explain the plot of the optical brightness of the thick BP sample in Figure 1d using the measured refractive indices. Because the BP sample is rather thick, the RGB values directly represent the averaged amounts of reflected light from the interface between air and BP layer in the corresponding spectral range. The abnormal feature in this figure is the contrary behavior of the R and G/B channels. For example, the R channel shows the minimum at ~0° (that is, the ZZ direction) and the maximum at 90° (AC), whereas the G/B channels are the maximums at 0° (ZZ) and minimums at 90° (AC). From Figure 4f, we can find that for the wavelength below 570 nm, which covers the B and G channels, n_{ZZ} is larger than n_{AC}, indicating stronger reflection for the G/B channels along ZZ (0°) than along AC (90°). For the wavelengths above 570 nm, n_{ZZ} is slightly smaller than n_{AC}, thus indicating stronger reflection for the R channel along AC (0°) than ZZ (90°).

CONCLUSIONS

We revealed the significant optical anisotropy of few-layer BP in the visible regime by using polarized optical microscopy and spectroscopy. Under linearly polarized white light illumination, the optical contrast in the RGB channels of few-layer BP on 300 nm SiO_2/Si exhibits the periodic variation when the sample was rotated. On the basis of this simple phenomenon, the crystalline orientation of BP can be easily identified. Moreover, for the first time, the anisotropic dielectric constant of 5 nm thick BP crystal was directly extracted using optical contrast spectra, on the basis of the classical electrodynamics and Fresnel equation. This technique can be used to measure the fundamental optical parameters of other anisotropic 2D crystals with atomic thickness and dozens of micrometer size. Our findings suggest that few-layer BP not only can be used as atomic-thick micro-optodevice in the visible regime such as linear polarizer, phase plate, and optical compensator but also is of great significance to a broad range of BP-related optoelectronic applications, making BP an ideal candidate for a light modulator with atomic thickness that can be integrated in optoelectronic and all-optical devices.

ASSOCIATED CONTENT

Supporting Information

The Supporting Information is available free of charge on the ACS Publications website at DOI: 10.1021/jacs.5b10685.

Angle-dependent contrast of few-layer black phosphorus (BP) on fused silica (Figure S1), high-resolution transmission electron microscope and atomic force microscope characterization (Figures S2 and S4), simulation results of angle-dependent optical contrast of BP on SiO_2/Si substrate (Figure S3), and comparison between the measured refractive index and the theoretical ones (Figure S5). (PDF)

AUTHOR INFORMATION

Corresponding Authors

*E-mail: tonglm@pku.edu.cn.

*E-mail: jinzhang@pku.edu.cn.

Notes

The authors declare no competing financial interest.

ACKNOWLEDGMENTS

J. Z. and L.T. acknowledge funding from NSFC (21233001, 21129001, 51272006, 51432002, 51121091, 11374355, and 21573004) and MOST (2011YQ0301240201 and 2011CB932601). K.L. acknowledges support from NSFC (11474006, 91433102, and 51522201) and National Program for Thousand Young Talents of China. We thank Jingming Zhang for the measurement of high-resolution transmission electron microscope.

REFERENCES

(1) Novoselov, K. S.; Geim, A. K.; Morozov, S. V.; Jiang, D.; Zhang, Y.; Dubonos, S. V.; Grigorieva, I. V.; Firsov, A. A. *Science* **2004**, *306*, 666.

(2) Geim, A. K.; Novoselov, K. S. *Nat. Mater.* **2007**, *6*, 183.

(3) Wang, F.; Zhang, Y.; Tian, C.; Girit, C.; Zettl, A.; Crommie, M.; Shen, Y. R. *Science* **2008**, *320*, 206.

(4) Splendiani, A.; Sun, L.; Zhang, Y.; Li, T.; Kim, J.; Chim, C.-Y.; Galli, G.; Wang, F. *Nano Lett.* **2010**, *10*, 1271.

(5) Jones, A. M.; Yu, H.; Ghimire, N. J.; Wu, S.; Aivazian, G.; Ross, J. S.; Zhao, B.; Yan, J.; Mandrus, D. G.; Xiao, D.; Yao, W.; Xu, X. *Nat. Nanotechnol.* **2013**, *8*, 634.

(6) Mak, K. F.; He, K.; Lee, C.; Lee, G. H.; Hone, J.; Heinz, T. F.; Shan, J. *Nat. Mater.* **2012**, *12*, 207.

(7) Geim, A. K.; Grigorieva, I. V. *Nature* **2013**, *499*, 419.

(8) Li, H.; Wu, J.; Yin, Z.; Zhang, H. *Acc. Chem. Res.* **2014**, *47*, 1067.

(9) Zhang, H. *ACS Nano* **2015**, *9*, 9451.

(10) Huang, X.; Zeng, Z.; Zhang, H. *Chem. Soc. Rev.* **2013**, *42*, 1934.

(11) Ling, X.; Wang, H.; Huang, S.; Xia, F.; Dresselhaus, M. S. *Proc. Natl. Acad. Sci. U. S. A.* **2015**, *112*, 4523.
(12) Churchill, H. O. H.; Jarillo-Herrero, P. *Nat. Nanotechnol.* **2014**, *9*, 330.
(13) Li, L. K.; Yu, Y. J.; Ye, G. J.; Ge, Q. Q.; Ou, X. D.; Wu, H.; Feng, D. L.; Chen, X. H.; Zhang, Y. B. *Nat. Nanotechnol.* **2014**, *9*, 372.
(14) Liu, H.; Neal, A. T.; Zhu, Z.; Luo, Z.; Xu, X. F.; Tomanek, D.; Ye, P. D. D. *ACS Nano* **2014**, *8*, 4033.
(15) Buscema, M.; Groenendijk, D. J.; Blanter, S. I.; Steele, G. A.; van der Zant, H. S. J.; Castellanos-Gomez, A. *Nano Lett.* **2014**, *14*, 3347.
(16) Wang, X.; Jones, A. M.; Seyler, K. L.; Tran, V.; Jia, Y.; Zhao, H.; Wang, H.; Yang, L.; Xu, X.; Xia, F. *Nat. Nanotechnol.* **2015**, *10*, 517.
(17) Zhang, S.; Yang, J.; Xu, R.; Wang, F.; Li, W.; Ghufran, M.; Zhang, Y.-W.; Yu, Z.; Zhang, G.; Qin, Q.; Lu, Y. *ACS Nano* **2014**, *8*, 9590.
(18) Hong, T.; Chamlagain, B.; Lin, W.; Chuang, H.-J.; Pan, M.; Zhou, Z.; Xu, Y.-Q. *Nanoscale* **2014**, *6*, 8978.
(19) Qiao, J.; Kong, X.; Hu, Z.-X.; Yang, F.; Ji, W. *Nat. Commun.* **2014**, *5*, 4475.
(20) Xia, F.; Wang, H.; Jia, Y. *Nat. Commun.* **2014**, *5*, 4458.
(21) Tran, V.; Soklaski, R.; Liang, Y. F.; Yang, L. *Phys. Rev. B: Condens. Matter Mater. Phys.* **2014**, *89*, 235319.
(22) Fei, R. X.; Yang, L. *Nano Lett.* **2014**, *14*, 2884.
(23) Low, T.; Rodin, A. S.; Carvalho, A.; Jiang, Y.; Wang, H.; Xia, F.; Castro Neto, A. H. *Phys. Rev. B: Condens. Matter Mater. Phys.* **2014**, *90*, 075434.
(24) Jiang, J.-W.; Park, H. S. *Nat. Commun.* **2014**, *5*, 4727.
(25) Wu, J.; Mao, N.; Xie, L.; Xu, H.; Zhang, J. *Angew. Chem., Int. Ed.* **2015**, *54*, 2366.
(26) Ling, X.; Liang, L.; Huang, S.; Puretzky, A. A.; Geohegan, D. B.; Sumpter, B. G.; Kong, J.; Meunier, V.; Dresselhaus, M. S. *Nano Lett.* **2015**, *15*, 4080.
(27) Ribeiro, H. B.; Pimenta, M. A.; de Matos, C. J. S.; Moreira, R. L.; Rodin, A. S.; Zapata, J. D.; de Souza, E. A. T.; Castro Neto, A. H. *ACS Nano* **2015**, *9*, 4270.
(28) Ge, S.; Li, C.; Zhang, Z.; Zhang, C.; Zhang, Y.; Qiu, J.; Wang, Q.; Liu, J.; Jia, S.; Feng, J.; Sun, D. *Nano Lett.* **2015**, *15*, 4650.
(29) Asahina, H.; Morita, A. *J. Phys. C: Solid State Phys.* **1984**, *17*, 1839.
(30) Morita, A. *Appl. Phys. A: Solids Surf.* **1986**, *39*, 227.
(31) Çakır, D.; Sahin, H.; Peeters, F. M. *Phys. Rev. B: Condens. Matter Mater. Phys.* **2014**, *90*, 205421.
(32) Yuan, H.; Liu, X.; Afshinmanesh, F.; Li, W.; Xu, G.; Sun, J.; Lian, B.; Curto, A. G.; Ye, G.; Hikita, Y.; Shen, Z.; Zhang, S.-C.; Chen, X.; Brongersma, M.; Hwang, H. Y.; Cui, Y. *Nat. Nanotechnol.* **2015**, *10*, 707.
(33) Yasaei, P.; Kumar, B.; Foroozan, T.; Wang, C.; Asadi, M.; Tuschel, D.; Indacochea, J. E.; Klie, R. F.; Salehi-Khojin, A. *Adv. Mater.* **2015**, *27*, 1887.
(34) Zhang, X.; Xie, H.; Liu, Z.; Tan, C.; Luo, Z.; Li, H.; Lin, J.; Sun, L.; Chen, W.; Xu, Z.; Xie, L.; Huang, W.; Zhang, H. *Angew. Chem., Int. Ed.* **2015**, *54*, 3653.
(35) Yim, C.; O'Brien, M.; McEvoy, N.; Winters, S.; Mirza, I.; Lunney, J. G.; Duesberg, G. S. *Appl. Phys. Lett.* **2014**, *104*, 103114.
(36) Liu, H.-L.; Shen, C.-C.; Su, S.-H.; Hsu, C.-L.; Li, M.-Y.; Li, L.-J. *Appl. Phys. Lett.* **2014**, *105*, 201905.
(37) Schubert, M. *Phys. Rev. B: Condens. Matter Mater. Phys.* **1996**, *53*, 4265.
(38) Delica, S.; Blanca, C. M. *Appl. Opt.* **2007**, *46*, 7237.
(39) Ni, Z. H.; Wang, H. M.; Kasim, J.; Fan, H. M.; Yu, T.; Wu, Y. H.; Feng, Y. P.; Shen, Z. X. *Nano Lett.* **2007**, *7*, 2758.
(40) Nolen, C. M.; Denina, G.; Teweldebrhan, D.; Bhanu, B.; Balandin, A. A. *ACS Nano* **2011**, *5*, 914.
(41) Roddaro, S.; Pingue, P.; Piazza, V.; Pellegrini, V.; Beltram, F. *Nano Lett.* **2007**, *7*, 2707.
(42) Casiraghi, C.; Hartschuh, A.; Lidorikis, E.; Qian, H.; Harutyunyan, H.; Gokus, T.; Novoselov, K. S.; Ferrari, A. C. *Nano Lett.* **2007**, *7*, 2711.
(43) Jung, I.; Pelton, M.; Piner, R.; Dikin, D. A.; Stankovich, S.; Watcharotone, S.; Hausner, M.; Ruoff, R. S. *Nano Lett.* **2007**, *7*, 3569.
(44) Gao, L.; Ren, W.; Li, F.; Cheng, H.-M. *ACS Nano* **2008**, *2*, 1625.
(45) Palik, E. D. *Handbook of Optical Constants of Solids*; Academic Press: New York, 1985.

DOI: 10.1021/jacs.5b10685
J. Am. Chem. Soc. 2016, 138, 300−305